

Article

X-ray Synchrotron Radiation to Look at Pigments in Antiquities: Overview and Examples

Alessandra Gianoncelli ¹, Sebastian Schöder ², Jasper R. Plaisier ¹, Maura Fugazzotto ³, Germana Barone ³,
Alfonsina Russo ⁴, Paolo Mazzoleni ³ and Simona Raneri ^{5,*}

¹ Elettra Sincrotrone Trieste, Strada Statale 14 km 163.5 in Area Science Park, Basovizza, 34149 Trieste, Italy; alessandra.gianoncelli@elettra.eu (A.G.); jasper.plaisier@elettra.eu (J.R.P.)

² Synchrotron SOLEIL, PUMA Beamline, L'Orme des Merisiers, Départementale 128, 91190 Saint-Aubin, France; sebastian.schoeder@synchrotron-soleil.fr

³ Department of Biological, Geological and Environmental Sciences, University of Catania, Corso Italia 57, 95129 Catania, Italy; maura.fugazzotto@unict.it (M.F.); germana.barone@unict.it (G.B.); paolo.mazzoleni@unict.it (P.M.)

⁴ Parco Archeologico del Colosseo, Piazza S.Maria Nova, 53, 00186 Rome, Italy; alfonsina.russo@cultura.gov.it

⁵ CNR-ICCOM, National Research Council, Institute of Chemistry of OrganoMetallic Compounds, Via G. Moruzzi 1, 56124 Pisa, Italy

* Correspondence: simona.raneri@pi.iccom.cnr.it; Tel.: +39-0506212678

Abstract: The recent upgrading of synchrotron radiation (SR) sources has favored, in the last few years, the construction and design of beamlines optimized for the study of cultural heritage materials, which may require ad hoc setups, specific spatial resolutions, and detection limits. In the field of cultural heritage, integrated approaches combining different techniques are often required, even at large facilities, where some beamlines offer the possibility of performing different types of measurements at the same point of analysis, complementing preliminary information usually obtained by conventional laboratory and/or portable in situ methods. An overview of the last ten years of synchrotron applications for the study of pigments is given, with discussion of upstream and downstream challenges to methods and techniques. The possibilities offered by the synchrotron techniques are illustrated by a case study of a particular class of painted ceramics, as an example of different research questions that are solved by a combination of SR-based methods.

Keywords: SR- μ XRF; SR- μ XANES; SR-XRD; pigments; ceramics



Citation: Gianoncelli, A.; Schöder, S.; Plaisier, J.R.; Fugazzotto, M.; Barone, G.; Russo, A.; Mazzoleni, P.; Raneri, S. X-ray Synchrotron Radiation to Look at Pigments in Antiquities: Overview and Examples. *Heritage* **2024**, *7*, 2118–2137. <https://doi.org/10.3390/heritage7040100>

Academic Editor: Maurizio Aceto

Received: 28 February 2024

Revised: 19 March 2024

Accepted: 31 March 2024

Published: 5 April 2024



Copyright: © 2024 by the authors. Licensee MDPI, Basel, Switzerland. This article is an open access article distributed under the terms and conditions of the Creative Commons Attribution (CC BY) license (<https://creativecommons.org/licenses/by/4.0/>).

1. Synchrotron for Cultural Heritages and Pigments Studies: Overview

1.1. Synchrotron Beamlines for Cultural Heritages in Europe

More and more, synchrotron beamlines are used for cultural heritage (CH) material characterization, enjoying nondestructiveness and high sensitivity at the microscale.

Over the last fifteen years, increasing attention has been paid to improving the performance of beamlines dedicated to cultural heritage, also taking advantage of the opening of new facilities (e.g., MAX IV laboratory, Lund, Sweden) or the upgrading of European facilities (e.g., from what has already been achieved at the European Synchrotron Radiation Facility (ESRF, France) to what is planned and announced for the future at Elettra (Italy) and SOLEIL (France)) (Table 1).

In addition to accelerator and instrument upgrades, the main challenges and improvements for scientific applications are focused on (i) the use of combinations of complementary techniques at a single site; (ii) the joint use of several beamlines at the same facility; (iii) the creation of a thematic network for accessing several facilities with a single proposal, also driven by new EU projects providing simultaneous access to multiple facilities (e.g., CERIC-ERIC, ReMAde@Ari, IPERION-CH/HS); (iv) the creation of new opportunities for improved experience in data analysis and data sharing (e.g., EXPANDS, PANOSC

EU-funded projects) [1–3]. In terms of measurements and data acquisition, for example, at ID21 beamline [4] of ESRF (which is regularly used for CH applications) in addition to the standard XRF mapping, the upgrade has enabled multi-edge analysis through XANES measurements; moreover, for micro-XRD mapping at ID21, the availability of fast pixel array detectors combined with fly-scan capability enables very rapid scans contrary to the past [1].

Table 1 displays an overview of the possibilities and capabilities for CH applications offered by European SR X-ray beamlines, shown in terms of available techniques, beam size, sample environment, and available energy range.

Table 1. List of European synchrotron X-ray beamlines suitable for cultural heritage (CH) applications, with the indication of available techniques and some practical and useful setup information.

Beamline	Facility	Country	Energy Range [keV]	Available Techniques	Beam Size [μm]	Sample Environment	Applications
PUMA	SOLEIL	France	7–22	μXRF , μXANES , μXRD	5×7	Air	CH (70%), other (30%)
LUCIA	SOLEIL	France	0.8–8	μXRF , μXANES	2×3	Vacuum	Life sciences, materials sciences, CH
Nanoscopium	SOLEIL	France	5–20	μXRF , μXANES	0.03–1	Air	Life sciences, materials sciences, environmental science, geobiology, CH
Psiche	SOLEIL	France	15–100	μCT	$1 \times 1^*$	Air	Geosciences, physics, chemistry, biology. CH
ID21	ESRF	France	2–11	μXRF , μXANES , μXRD	0.03×0.07	Vacuum	Life sciences, materials sciences, CH
ID16B	ESRF	France	6–65	μXRF , μXANES , μXRD	0.05×0.05	Air	Life sciences, materials sciences, CH
ID22	ESRF	France	6–80	XRD, μXRD	50×50 – 2000×1000	Air	Chemistry, physics, engineering, CH
ID13	ESRF	France	7–30	μXRF , μXRD , SAXS	0.1×0.1 – 20×20	Air	Materials sciences, physics, engineering, CH
TwinMic	Elettra	Italy	0.2–2.2	μXRF , μXANES , STXM	circular, diameter from 0.1 to 2.5	Vacuum	Life sciences, materials sciences, CH
X-ray Fluorescence	Elettra	Italy	2–15	μXRF , μXANES ,	100–200	Vacuum	Life sciences, materials sciences, CH
MCX	Elettra	Italy	6–20	μXRD	300–2000	Air	Life sciences, materials sciences, CH
Esca Microscopy	Elettra	Italy	90–1200	SPEM, XPS	0.1–0.2	Vacuum	Life sciences, materials sciences, CH

Table 1. Cont.

Beamline	Facility	Country	Energy Range [keV]	Available Techniques	Beam Size [μm]	Sample Environment	Applications
XAFS	Elettra	Italy	2.4–25	XAS, XANES	2000	Air	Life sciences, materials sciences, CH
SYRMEP	Elettra	Italy	9–40	μCT	0.9 *	Air	Life sciences, materials sciences, CH
I08	Diamond	UK	0.2–4.2	μXRF , μXANES , STXM	circular, diameter from 0.1 to 2	Vacuum, cryostat	Life sciences, materials sciences, CH
I13	Diamond	UK	8–30	μCT	0.05	Air	Life sciences, materials sciences, CH
I14	Diamond	UK	5–23	XRF, XRD, XANES mapping, ptychography	0.05	Air	Life sciences, materials sciences, CH
I18	Diamond	UK	2–20.7	XAS-CT, XRD-CT, XAS/XRF, XRD/XRF	2×2	Air or helium enclosure, He/N ₂ cryostat, sample heating	Life sciences, materials sciences, CH
B18	Diamond	UK	2–35	XAS/XRD, XAS/DRIFTSXAS/Raman, XAS/UV-Vis	200×250	Air	Life sciences, materials sciences, CH
NanoMAX	MAXIV	Sweden	6–28	μXRF , μXANES , ptychography	0.05 to 0.2	Air	Life sciences, materials sciences, CH
SoftiMAX	MAXIV	Sweden	0.275–2.5	μXRF , μXANES , STXM	0.01 to 0.1	Vacuum	Life sciences, materials sciences, CH
P06	DESY	Germany	8–30	nanoXRF, XAS, XRD, ptychography	0.05–0.1	Air	Life sciences, materials sciences, CH
P05	DESY	Germany	5–50	μCT	≤ 0.1 *	Air	Life sciences, materials sciences, CH

* Achievable spatial resolution.

1.2. X-ray Synchrotron Techniques for Pigments Studies

The characterization of pigments and painting techniques is of great importance in the CH field, from authentication to provenance issues, from conservation to restoration. Studying unique artefacts can impose constraints on how samples are taken and handled, sometimes limiting the information that traditional laboratory analysis can provide. Preserving the integrity of precious specimens and obtaining clear compositional information from decorated surfaces can be challenging, even when using well-established techniques for characterizing and analyzing ancient materials. X-ray spectroscopy methods at synchrotron radiation facilities are increasingly being used to analyze cultural heritage materials such as pigments and decorated artefacts. These materials are often characterized

by complex stratigraphy and/or heterogeneous material compositions [5–9]; the possibility of using a combination of techniques to study different aspects, namely, characterization, degradation, and material changes, is highly recommended.

X-ray fluorescence spectroscopy (XRF) is one of the most widely used techniques, allowing mapping of the distribution of chemical elements and their colocalization at the micro- and sub-microscale, with micro- or nanofocused beams [10,11]. In addition, under specific conditions, it allows quantitative determination [12–14].

As mentioned above, when dealing with complex systems, combining different analytical techniques is essential and can provide complementary information. In this context, synchrotron radiation X-ray diffraction (SR-XRD) is commonly used for phase identification and crystal structure determination [15,16]. This method is frequently used to reveal the stratigraphy of painted objects and allow profile studies in specific configurations, such as the grazing incidence mode [17], or to identify degradation products on the painting surface.

SR-XRD and SR-XRF are also used in combination with SR-micro-X-ray absorption near-edge structure (SR- μ XANES), which is fundamental for the investigation of alteration mechanisms involving redox processes [18–20]. Using focused beams, this method can reveal the oxidation state and local ordering of selected elements on the micro- and nanoscales.

Over the last decade, various examples of the use of synchrotron-radiation-based methods for the analysis of pigments have been increasingly reported in the scientific literature. This has enriched the discussion regarding the upstream and downstream challenges for analyzing CH materials at synchrotron facilities.

1.3. Pigments in Archaeological Artifacts: From Rock Art to Potteries

SR-based methods have been proven to be particularly suitable for characterizing pigments in wall paintings and rock art [21], sometimes in combination with in situ investigations [22] and traditional laboratory-based analyses on microsamples [23,24]. In detail, chemical and mineralogical SR-based techniques (e.g., SR- μ XRF, synchrotron radiation macro X-ray fluorescence (SR-MA-XRF), SR- μ XANES; SR- μ XRD) have been successfully employed in identifying minor phases and obtaining important crystallographic data separating anthropogenic markers and post-depositional processes [21] and to reveal the relationship between the physicochemical properties (e.g., crystallinity, morphology, surface density) and the color in iron-oxide-based decorations in caves [22–25] as well as to determine iron-oxide-based compounds present in small quantities that are quite difficult to detect with classical methods on intonaco [26]. The SR- μ XRD technique has also been used to distinguish original from repainted rock art [21] and to identify the nature of pigments on prehistoric ceramic decorations [27], where the characterization of Fe- and Mn-based compounds is not straightforward and the use of advanced methods becomes fundamental [28].

1.4. Pigments in Glazes

The characterization of pigments in glazed and painted ceramics by X-ray techniques, especially using conventional laboratory equipment, is crucial when investigating technological aspects [29].

SR- μ XRD has been largely used to characterize crystalline compounds of tin and lead glazed ceramics, majolica, and porcelain and to reveal relevant technological information. Pradell et al., 2018 [30], employed SR- μ XRD combined with synchrotron extended X-ray absorption fine structure (SR-EXAFS) and SR-XANES to identify technological aspects such as firing conditions in luster ceramics, observing the correlation with the obtained microstructure and optical effects of the surfaces. Molera et al., 2022 [31], used in situ SR-XRD to identify the sequence of manganese compounds developed during firing in high-lead glass; time/temperature-resolved SR-XRD was used to understand manufacturing issues in glazed colored ceramics; in particular, the historical processing of cobalt arsenide ore used for blue decorated glazes was investigated [32].

Numerous experiments have been focused on identifying the mineralogical nature of microcrystallites phases within glazed layer on thin sections of lead glazed ceramics and glazed tiles (for example on the colored Portuguese azulejos) by using synchrotron through-the-substrate X-ray microdiffraction (tts-XRD) [33–36].

SR-XANES at the Fe K-edge [37], Cu K-edge [30,38], Cr K-edge [39], Co K-edge [29,40], Mn K-Edge [37], and As K-edge [41] has been demonstrated to be a powerful method in studying the elemental precursors of the glaze's color (thus identifying the speciation of colorant ions), for obtaining information both on technology and provenance in various glazed ceramic manufactures (e.g., porcelains).

The production process of brown glazed porcelain has been studied by SR-EXAFS in order to clarify the coloring mechanism [42]; both SR-XANES and SR-EXAFS enabled investigating the glass nanostructure of blue glaze in stonewares, explaining their particular colorful aspect [43].

Where the determination of the distribution and colocalization of chemical elements is critical, the use of scanning SR- μ XRF is of great importance, for example, in the study of glaze layers to map the distribution of dyes and/or specific elements in Chinese porcelain [29,40,44], Attic, and western-Greek black-glazed vessels [45] and ancient black-glazed wares [46].

1.5. Ink, Dyes and Organic Colorants

Inks used for papyri and ancient manuscripts have been studied using SR-based techniques to improve knowledge of their recipes and raw material provenance. This has also been combined with laboratory-based techniques [47]. Christiansen et al., 2017, 2020 [48,49], explored the composition of red and black inks in papyri by SR-MA-XRF and SR-XANES, while Autran et al., 2021 [50], studied carbon black inks on papyri by means of SR-XRD and SR-XRF, and investigated the production process of the inks by means of integrated synchrotron X-ray diffraction and X-ray fluorescence computed tomography (SR-XRD-CT and SR-XRF-CT).

The application of the multianalytical approach has been demonstrated to be fundamental in disclosing raw materials used for inks on papyri [48–50], pigments on ancient manuscripts [51], hidden text on papyri [52], and on degraded manuscripts [53]. Information on the origin of the pigments can also be obtained [51].

In addition to the studies on written supports, the application of SR-based X-ray studies on colored textiles seems to be of particular interest; for example, Späth et al., 2021 [54], used SR- μ XRF imaging to detect the distribution of metal organic pigments within individual fibers of an ancient Siberian pile carpet.

1.6. Paintings: Pigments Characterization and Degradation Products

SR-based techniques are commonly used to identify the main components of paint, namely, pigments and coating, and to study degradation processes [55–57]. Fading, darkening, and bleaching are just a few examples of color changes due to photodegradation of pigments. Apart from the nature of the pigment, these changes depend on a series of complex interactions between pigment–binder–support, as well as exposure and/or conservation conditions [58]. In fact, synchrotron-based X-ray methods have been widely and successfully used to better understand the chemical transformations involved in the natural degradation of artists' pigments in paintings (mainly oil paints) [5,59–66].

Specifically, SR- μ XRD, SR- μ XRF mapping, and SR-XANES on Cr/S/Cl K-edge and Cd L3-edge have been used for investigating the degradation of chrome yellow and cadmium sulfide in oil paints, in some cases together with complementary techniques such as SR- μ Raman and SR- μ FTIR [18,59,65]. The unclear degradation process of As-based pigments in tempera paintings has been explored by using SR- μ XRD, SR- μ XRF and SR-XANES on S K-edge, As K-edge, and Ag L3 K-edge [18]. SR- μ XANES on Cr K-edge mapping has been used to study alterations on potassium chromate paints [67], and, together with SR- μ XRF, to study lead-chromate-based pigments in oil paints [60]. SR-XANES on S K-edge has been

proven to be useful in the investigation of technological issues related to blue pigments and their shades, e.g., in ultramarine blue [68].

To study the discoloration mechanisms of synthetic ultramarine blue, SR-XANES focused on Al K-edge has been used [69], suggesting an increase in the S^{3-} radicals with prolonged exposure. Blue pigments, both in tempera and in oil paints, have been furthermore investigated by means of SR-XRD, together with SR- μ FTIR, to identify their composition and the related alteration compounds [66], e.g., the correlation between the size of the pigment particles and the darkening of the surface due to the easier encapsulation of environmental dust on the porosity of the pigment layer. Moreover, SR-XRD has also been utilized to obtain specific information on the preparation of raw materials and the post-treatment of lead white pigments in easel paintings. This information has provided clues to pigment quality (e.g., by studying the hydrocerussite: cerussite ratio or crystallite dimensions) [57,70].

In addition to the studies carried out on historical paintings, a number of studies have been carried out on laboratory replicas in order to better understand the parameters responsible for the degradation mechanisms, such as the influence of the binding medium on arsenic sulfide pigments studied by Vermeulen et al., 2018 [71] with SR- μ XANES on S K-edge.

SR-XRD is commonly used for the pigments characterization on oil paintings [56], but it was also involved in a large multianalytical approach, for example, to define a specific protocol identifying glauconite and celadonite within green earth pigments [72].

SR-based X-rays techniques, such as SR-XRF mapping, have been demonstrated to be fundamental during conservation treatments, helping in the control of the interventions as well as in the revealing of features that were not visible on the degraded surface of the paint [73].

Lastly, SR-based X-rays techniques (e.g., SR- μ XRD, SR- μ XRF, SR- μ XANES, SR- μ FTIR and SR-MA-XRF, and SR-MA-XRD) have also been utilized to test new protocols of embedding painting microsamples [74], as well as for authentication studies [75,76]. They appear to be useful, furthermore, in the identification of pigments' mixtures and in complex stratigraphic artworks [77]. A comprehensive review on SR-MA-XRF's applications, and its use in comparison with other techniques, is offered by Alfred et al. [78].

1.7. Pigments and Radiation Damage

In the cultural heritage field, technological advances tend to optimize portable equipment to minimize the information to (risk of) damage ratio, i.e., to obtain the maximum information with the minimum manipulation or risk to the objects [79]. Overall, it is essential that the sample is not destroyed, to allow further analysis. Therefore, when using intense radiation sources such as synchrotron light, the potential damage to samples should be taken into account seriously. Depending on the irradiation parameters, the properties of the studied materials and the environmental factors, so-called nondestructive, high-brilliance techniques, can cause undesirable physical or chemical changes in the objects, sometimes even visible to the naked eye [65,80,81]. Recent studies have focused on developing analytical strategies and instruments to detect or mitigate the effects of irradiation on cultural heritage samples [81]. Some authors, instead, proposed suggestions related to the sequence of analytical techniques to apply on a sample, in order to avoid loss of information. For instance, Ghirardello et al., 2022 [65], recommend the use of micro-PL before SR- μ XRD, which can determine darkening of the sample surface, that may obscure the subsequent PL response.

Godet et al., 2022 [82], illustrated the X-rays effect on blue and green Egyptian pigments, highlighting the different sensitivity of the two pigments to increasing doses of irradiation by using EPR spectroscopy; Monico et al., 2020 [62], examined the damages induced by synchrotron radiation-based X-ray microanalysis on chrome yellow paints; Gervais et al., 2015 [83], investigated those induced in Prussian blue and zinc white pigments on historical paints. Ion and X-rays-induced effects were studied by Carrasco et al., 2018 [84], on azurite, malachite, and alizarin pictorial replicas; Ganio et al., 2018 [68],

exposed a first assessment on the acceptable amount of radiation exposure with XANES investigation to define the optimal acquisition parameters to allow safe analyses of lapislazuli and ultramarine pigments.

2. Painted Architectural Terracottas: A Meaningful Example of Integrated Approach

Among painted ancient objects, decorated ceramics may present problems of authentication or interpretation (e.g., objects recovered by requisition, evidence of cultural change, identification of painting workshops, etc.). In such cases, where sampling is limited and questions are multiple, routine laboratory or portable in situ techniques may leave unresolved questions (such as identifying crystalline phases or oxide speciation), and further progress in knowledge can be ensured by applying advanced noninvasive methods.

In the present study, two sets of materials, namely, architectural slabs from Cerveteri involved in a case of antiquities requisition [85] and decorated architectural terracottas from the Palatine Hill in Rome [86], were studied using SR-based X-ray methods to solve characterization problems that were not readily achievable using traditional nondestructive and noninvasive analytical techniques, such as portable Raman spectroscopy and X-ray fluorescence spectroscopy (Figure 1). Microsamples of pictorial layers were sampled by using a scalpel and analyzed by integrating and exploiting the possibilities offered by two different beamlines particularly suitable for CH materials at two different facilities, namely, the French Synchrotron SOLEIL and the Italian facility ELETTRA. In particular, the samples were analyzed at the cultural heritage dedicated PUMA beamline [45] (SOLEIL Synchrotron, Saint-Aubin, France) by means of XRF elemental mapping and XANES spectroscopy for speciation of Fe- and Mn-based layers, and at MCX beamline [87] (Elettra Sincrotrone Trieste, Trieste, Italy) with the XRD technique.

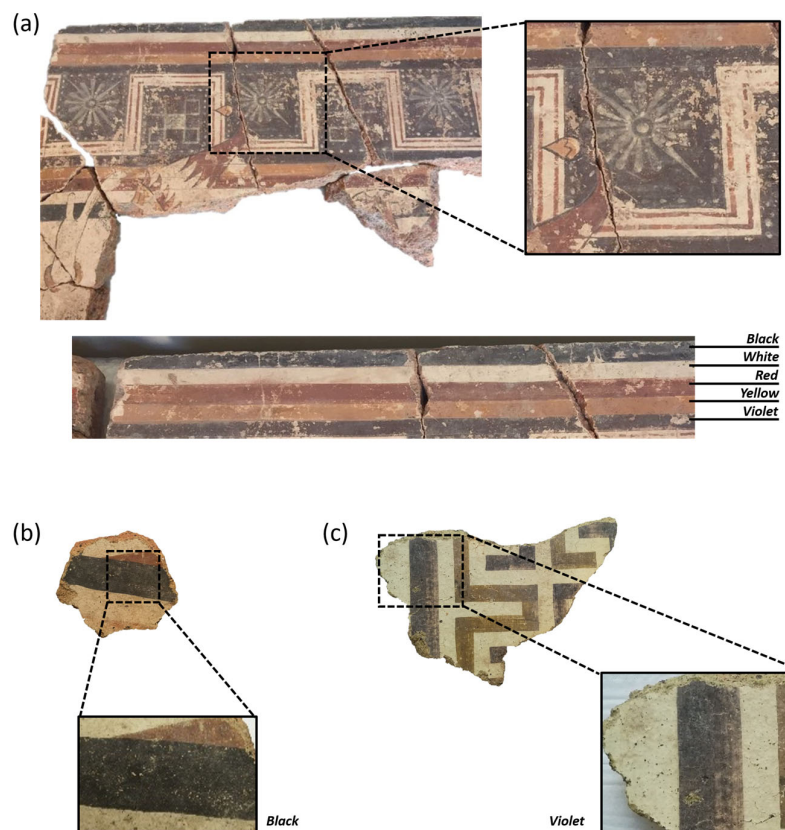


Figure 1. (a) Example of painted terracotta from Cerveteri—slab L11 and details of painted areas showing the colors investigated: violet, black, white, red, and yellow; (b) example of painted terracotta from Palatine Hill—slab Pal13 and detail of the black tint investigated; (c) example of painted terracotta from Palatine Hill—slab Pal12 and detail of the violet tint investigated.

2.1. Materials and Methods

The first group of analyzed specimens consists of fragments of painted architectural terracotta samples from Cerveteri, recovered from a requisition carried out by the Italian authorities in 2016 during one of the most important investigations into the illicit trafficking of antiquities in recent decades [85,88]. The second group consists of fragments of polychrome painted architectural terracotta found in the Palatine and Roman Foro in Rome, now preserved in the Colosseo Archaeological Park. They are unique pieces dating to the Late Archaic period (5th century BC), the production of which may be linked to both Etruscan and Roman workshops [86], characterized by polychrome decorated surfaces with tones and motifs similar to the Etruscan terracottas from Cerveteri [85,89,90]. Samples were taken from selected areas of the slab fragments. The slabs were in a good state of preservation; some had been restored to remove secondary precipitation phases [85]. In total, twelve microsamples from Cerveteri slabs (four black, three violet, three green/grey) and seventeen from Palatine Hill slabs (three black, one blue, two violet, seven red) were examined, selected to be representative of the color range observed on the architectural terracottas. Exploratory laboratory and in situ XRF and Raman analyses provided the basis for advanced investigations at synchrotron sources [85,86].

Samples were examined at the cultural heritage dedicated PUMA beamline [45] SOLEIL Synchrotron (Saint Aubin, France), where a KB mirror focuses the monochromatized X-ray photons into a spot of $5\ \mu\text{m} \times 7\ \mu\text{m}$ on the sample plane. The measurements are performed in ambient air and room temperature. The XRF signal is acquired by an SGX Sirius SD silicon drift detector installed at 90° from the incident beam. A visible light microscope located perpendicularly to the sample surface allows micrometric visualization and navigation of the sample. During our XRF mapping, the samples were scanned at 18 keV with a step size of $10\ \mu\text{m}$ using 0.5 s acquisition time per pixel. A flat area on the samples' surface was selected and scanned in order to obtain reliable results and avoid spectral "artifacts" due to surface microroughness or morphological issues.

After XRF mapping, XANES spectra were collected on black and violet Mn-based layers in fluorescence mode, in specific microspots with 1 s/point acquisition time. For Fe K-edge, an energy resolution of 2 eV was chosen in the pre-edge range from 7.05 to 7.11 keV and in the post-edge zone from 7.16 to 7.4 keV. The area around the edge from 7.11 to 7.16 keV was scanned with higher energy resolution, in steps of 0.5 eV. For Mn K-edge, an energy resolution of 2 eV was used in the pre-edge range from 6.5 to 6.53 keV and in the post-edge range from 6.65 to 6.8 keV, while close to the edge from 6.53 to 6.65 KeV with an energy resolution of 0.5 eV/step.

XRD diffraction patterns were acquired at MCX beamline [87] of the ELETTRA-Synchrotron facility (Trieste, Italy). The powder patterns were collected in reflection mode, with an incident angle of about 5° . The samples were aligned to the incoming beam using a laser interferometer. Data were collected at room temperature using a monochromatic wavelength of $0.8266\ \text{\AA}$ (15 keV), on a 4-circle Huber goniometer equipped with a scintillation detector in the $5\text{--}50^\circ$ 2θ angular range with a 0.01 step size and 0.5 s counting time. The experimental diffraction patterns were confronted with patterns present in the PDF-4 database using the program Sieve [91].

For both the PUMA and MCX beamlines, no sample preparation is required: measurements are made on the samples' surface, selecting areas that are as flat as possible according to the incident beam.

2.2. Results and Discussion

2.2.1. The Case of the Manganese-Black Technique

The available literature on black decorations on Etruscan architectural terracottas carried out using routine laboratory or portable methods [86,88–90] indicate the use of Fe- and Mn-based pigments; different interpretations are proposed, namely, the use of manganese-black technique [92] or the use of natural pigments based on manganese and iron oxides [93]. The advantage of the manganese black technique lies in the possibility of

obtaining the red and black color in a single oxidizing firing cycle, starting from a mixture of Fe-Mn oxides (probably hematite and pyrolusite) that forms a stable spinel-like phase, namely, jacobite (MnFe_2O_4). In the past, different Mn oxides and hydroxides have been used to decorate artefacts; in these phases, manganese can have different oxidation states, which in turn depend on technical issues, especially firing conditions. Correctly characterizing or identifying manganese oxides by Raman spectroscopy can be complex [94,95]. Recent systematic studies on Mn oxides, incorporating a variety of methods, have additionally proposed valid approaches to solve identification problems by Raman spectroscopy [96]. However, it is necessary to consider the possible degradation of the sample due to the laser power and the difficulties of analyzing highly inhomogeneous samples in the absence of accurate mapping systems, which are sometimes difficult to obtain directly in situ or on microsamples.

In the study of chemical element speciation in mineral compounds, SR- μ XRF mapping is a necessary step in the process to locate the distribution of chemical elements of interest and, thus, the areas over which absorption spectra can be collected.

In Figure 2a–c, SR- μ XRF mapping of black pigments from Cerveteri and Palatine Hill shows the distribution of iron and manganese on the decorated pictorial layers; in the majority of the samples, manganese, present in the pigment layer, seems to be localized on the colored surface together with iron, which mainly comes from the background; on some spots pertaining to the pigment layers, Fe-Mn colocalization can be observed. SR- μ XANES spectra at the Fe K-edge and Mn K-edge can, thus, be collected on the detected Fe and Mn spots. Looking at the SR- μ XANES spectra (see Figure 2d,e), the pre-edge, post-edge, and edge features are slightly shifted with respect to the selected reference phases, namely, Mn-oxides (pyrolusite (MnO_2), bixbyite (Mn_2O_3), and Fe-Mn spinel phases (jacobite, MnFe_2O_4). In some cases, the pre-edge structure appears to correspond to hausmannite or jacobite (e.g., Pal1 and L16), while the edge position and post-edge features are more closely related to pyrolusite. The not-perfect correspondence with reference Mn-based mineral phases selected as standards among those commonly found in archaeological materials [94] might be clarified by means of complementary SR- μ XRD studies. In fact, in the case under consideration, SR- μ XRD showed the presence of Mn-Fe spinel in all the black layers studied (Table 2, Figure 3); in some cases, iron and manganese oxides are still present as hematite and bixbyite, suggesting an incomplete transformation of the Fe and Mn oxide mixture, which depends on the firing temperature and the ratio of the two oxides in the raw material [92].

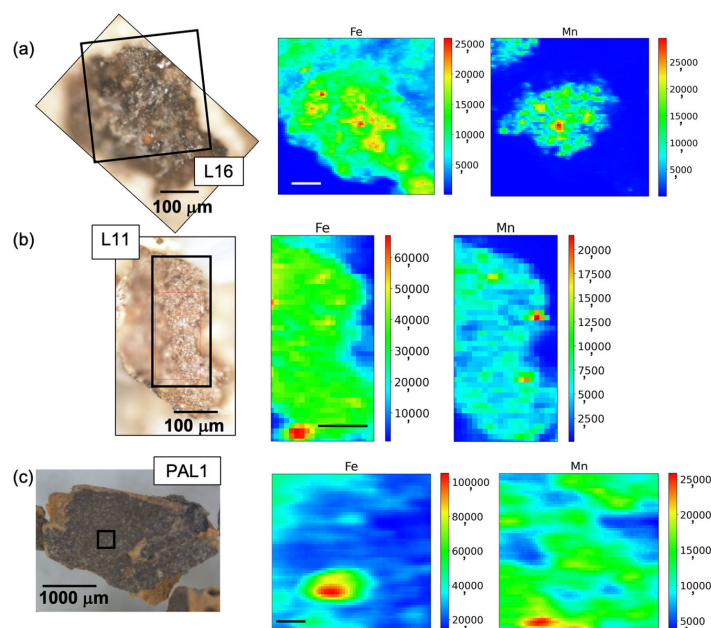


Figure 2. Cont.

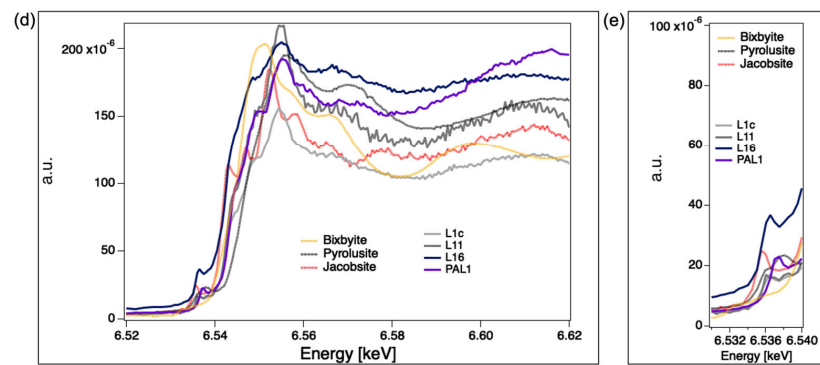


Figure 2. (a–c) Example of black layers (L11, L16, and Pal1) at microscope investigation and corresponding Fe and Mn maps (scale bars are 50 μm) collected over an area of $300 \times 300 \mu\text{m}^2$ with 1 s acquisition time per pixel; (d,e) μXANES spectra collected on Fe K-edge and Mn K-edge on black spots. The black boxes on the visible images indicate the areas mapped by XRF.

Table 2. Mineralogical phases detected by SR- μXRD at the MCX-Elettra Synchrotron Facility previously analyzed at the PUMA-Soleil Synchrotron Facility. In bold are mineral phases attributable to black pigments; the other mineral phases can be related to the painted architectural slabs, including clays, inclusions, and new-forming minerals.

Sample ID	Mineralogical Phases (in Order of Relative Abundance)
L1c	Quartz, anorthite (Na-bearing, disordered), melilite, Mn-Fe spinel (jacobsite; $[\text{MnFe}]_2\text{O}_4$) , clay minerals (illite, ?).
L9	Quartz, anorthite (Na-bearing), hematite, Mn-Fe spinel (jacobsite; $[\text{MnFe}]_2\text{O}_4$) , bixbyite (Mn_2O_3).
Pal1	Quartz, Mn-Fe spinel (jacobsite; $[\text{MnFe}]_2\text{O}_4$) .
Pal3	Mn-Fe spinel (jacobsite; $[\text{MnFe}]_2\text{O}_4$) , quartz.
Pal13	Quartz, calcite, Fe-Mn spinel (jacobsite; $[\text{MnFe}]_2\text{O}_4$) , gehlenite.

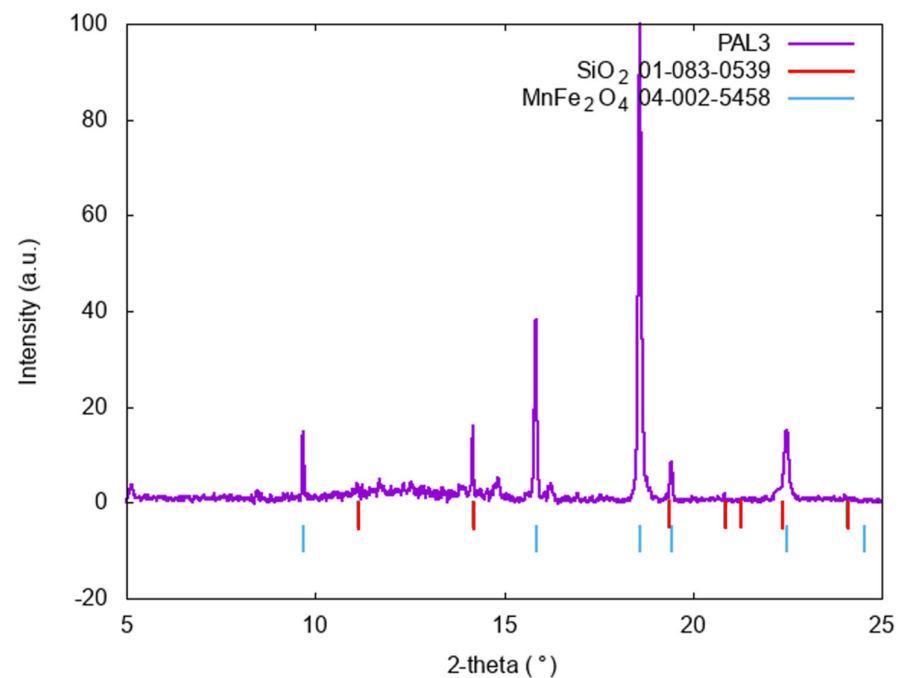


Figure 3. SR- μXRD pattern collected at the MCX-Elettra Synchrotron Facility on sample Pal3, as an example of black pigments.

2.2.2. Looking at Pigment Grains: Stratigraphies or Mixtures of Hues?

An important example of mixing vs. superimposing layers is the case of purple layers in Etruscan painted terracotta; in fact, in the literature, the superimposition of layers has been suggested as a way of producing purple layers, namely, using azurite on red-hematite-based layers, as in the famous Etruscan slab from Guerriero di Ceri [88]. However, studies of wall paintings in Etruscan tombs in Tarquinia have shown a great variability in the production of violet layers, including the use of cinnabar, Tyrian purple, or red ochre [89].

In the examined case study, preliminary investigation of the violet pigments ruled out the presence of microstratigraphy. Instead, it revealed the presence of both red and black grains, for which the identity of the darker spots requires further investigation [89]. SR- μ XANES spectra at the Mn K-edge (Figure 4d) collected on black grains show a pre-edge and an edge energy consistent with pyrolusite, while μ XANES at the Fe-edge (Figure 4e) on red grains clearly show a pre-edge at energies of hematite, when compared to Fe²⁺, Fe³⁺, and Fe-mixed references. SR- μ XRF maps show, furthermore, that the two elements are localized in different areas of the pictorial layer (Figure 4a,b). The SR- μ XRD analysis reveals the presence of both hematite and pyrolusite, while in some cases also identifying Fe-Mn spinel (Table 3, Figure 5). Looking at the relationship between the violet areas and the decorative motif, it is plausible that violet had been deliberately obtained with specific mixtures that give back a violet shade, where hematite is associated with both pyrolusite and Fe-Mn spinel.

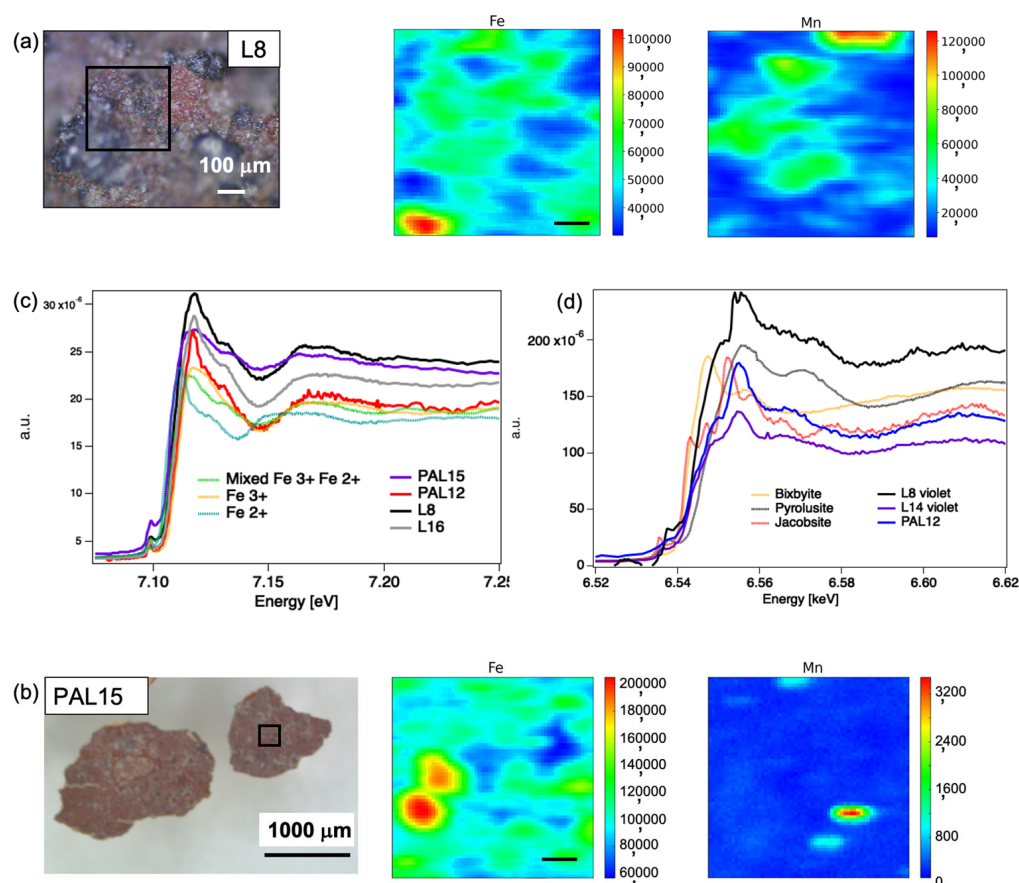


Figure 4. (a,b) Example of violet layers (L8 and Pal15) at microscope investigation with corresponding Fe and Mn maps (scale bars are 50 μ m) collected on an area of $300 \times 300 \mu\text{m}^2$ with 1 s acquisition time per pixel; (c,d) μ XANES spectra collected at Fe K-edge and Mn K-edge on red and black spots, respectively, on different violet samples. The black boxes on the visible images indicate the areas mapped by XRF.

Table 3. Mineralogical phases detected by SR-XRD at the MCX-Elettra Synchrotron Facility previously analyzed at the PUMA-Soleil Synchrotron Facility. In bold are mineral phases attributable to violet pigments; the other mineral phases can be related to the terracottas, including clays, inclusions and new-forming minerals.

Sample ID	Mineralogical Phases (in Order of Relative Abundance)
L14	Quartz, gypsum, illite, hematite, pyrolusite.
L16	Albite (Ca-bearing), quartz, gehlenite, Fe-Mn spinel.
Pal12	Calcite, Fe-Mn spinel , melilite.
Pal15	Hematite, MnOx (pyrolusite, MnO₂, ?).

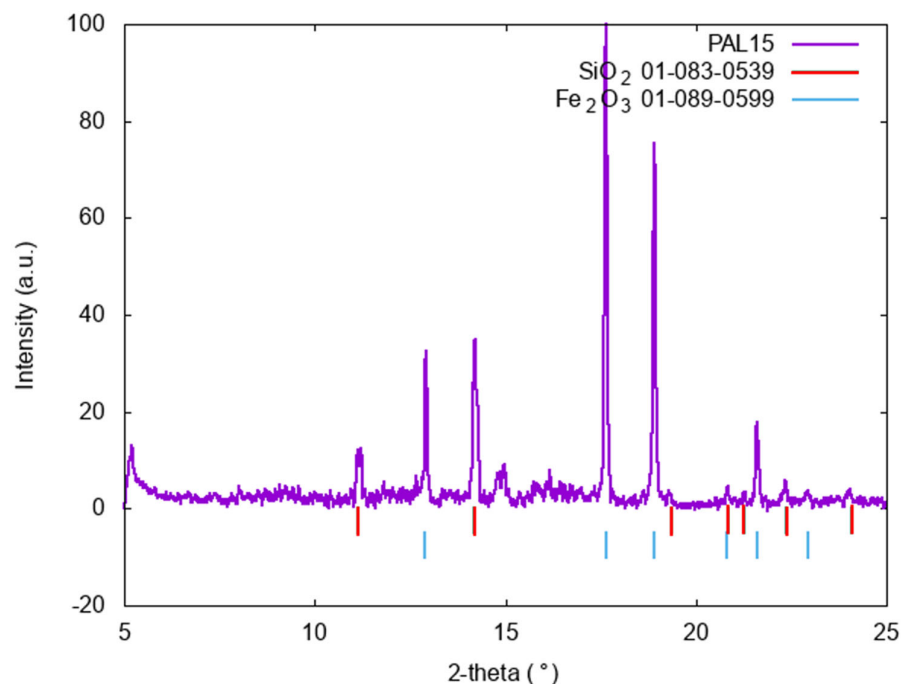


Figure 5. SR-XRD pattern collected at the MCX-Elettra Synchrotron Facility on sample Pal15, as an example of violet pigments. Diffraction pattern on the red grains.

2.2.3. SR- μ XRD for Solving Ambiguities: The Case of Blue and Green Pigments

Traditional noninvasive and nondestructive Raman and XRF methods are not always straightforward for the investigation and characterization of green and blue pigments [97–99]. The combination of SR-XRD and SR- μ XRF data may provide insight. Spectrochemical and diffraction data maps collected on green and blue pictorial layers from Cerveteri slabs (Figures 6 and 7) demonstrate the need to integrate different methods to obtain unambiguous results; in the case of green surfaces, chemical maps would suggest the use of green earth (mixture of hydrosilicate of Fe, Mg, Al, K) mixed with pyrolusite to darken the color, as confirmed by the presence of Mn-oxides from XRD data (Figure 8a), while Egyptian blue is clearly detected by XRD patterns and by colocalization of Ca and Cu in chemical maps (Figure 8b).

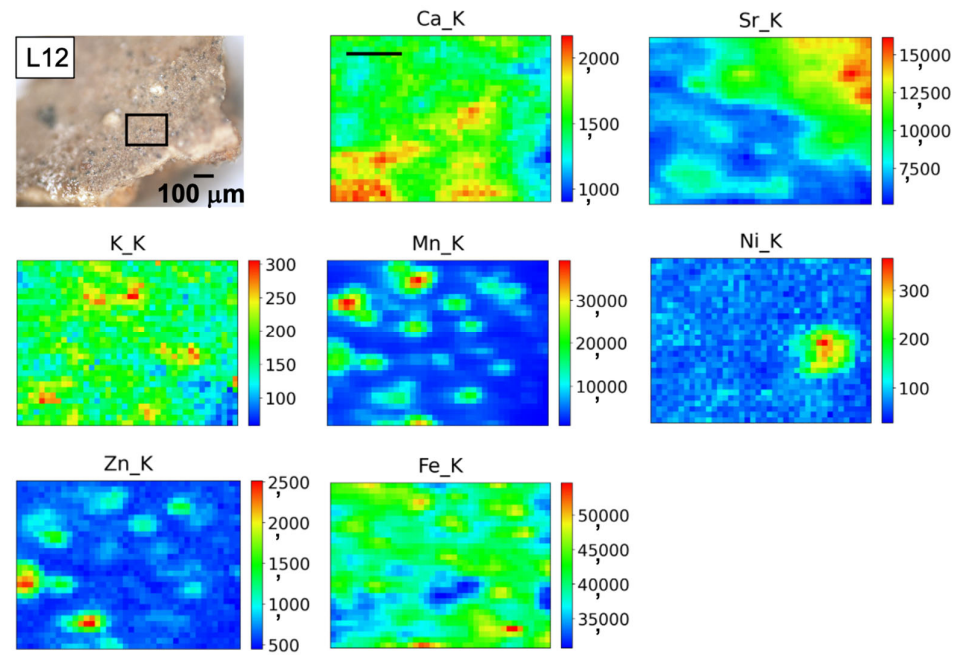


Figure 6. Example of green layer (L12) at optical microscope investigation and corresponding XRF maps of Ca, K, Mn, Sr, Ni, Zn, and Fe collected at 18 keV over an area of $200 \times 150 \mu\text{m}^2$ with 1 s acquisition time per pixel. Scale bars are 50 μm. The black box on the visible image indicates the area mapped by XRF.

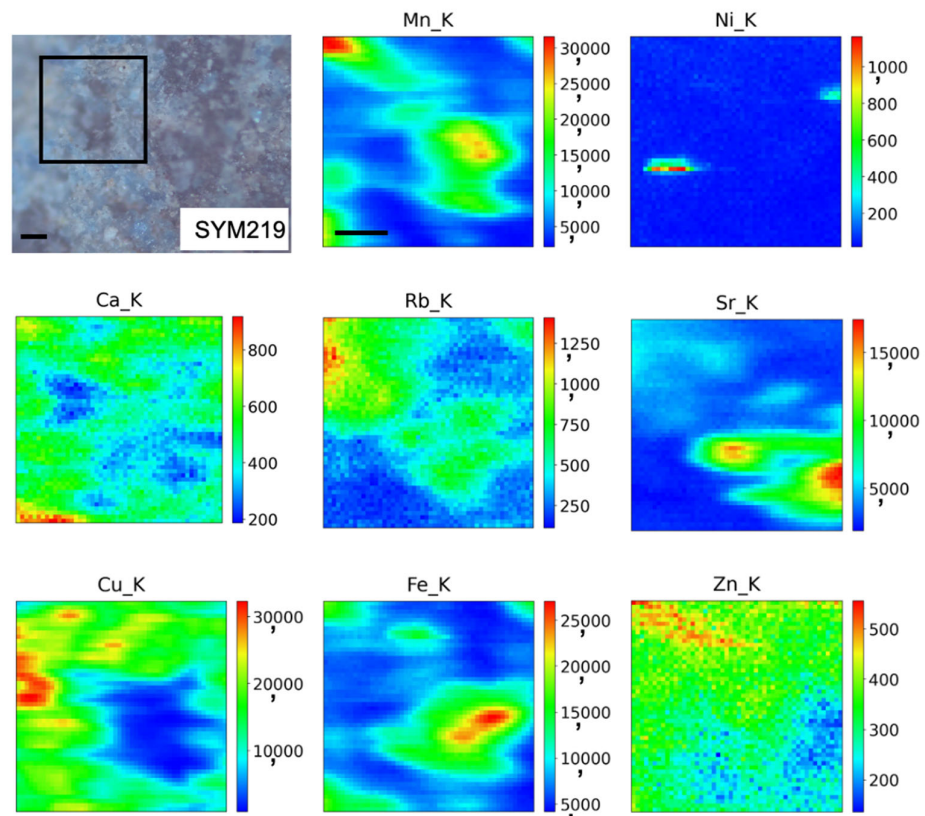


Figure 7. Example of blue layer (SYM219) at optical microscope investigation and corresponding XRF maps of Mn, Ni, Ca, Rb, Sr, Cu, Fe, and Zn collected at 18 keV over an area of $200 \times 200 \mu\text{m}^2$ with 1 s acquisition time per pixel. Scale bars are 50 μm. The black box on the visible image indicates the area mapped by XRF.

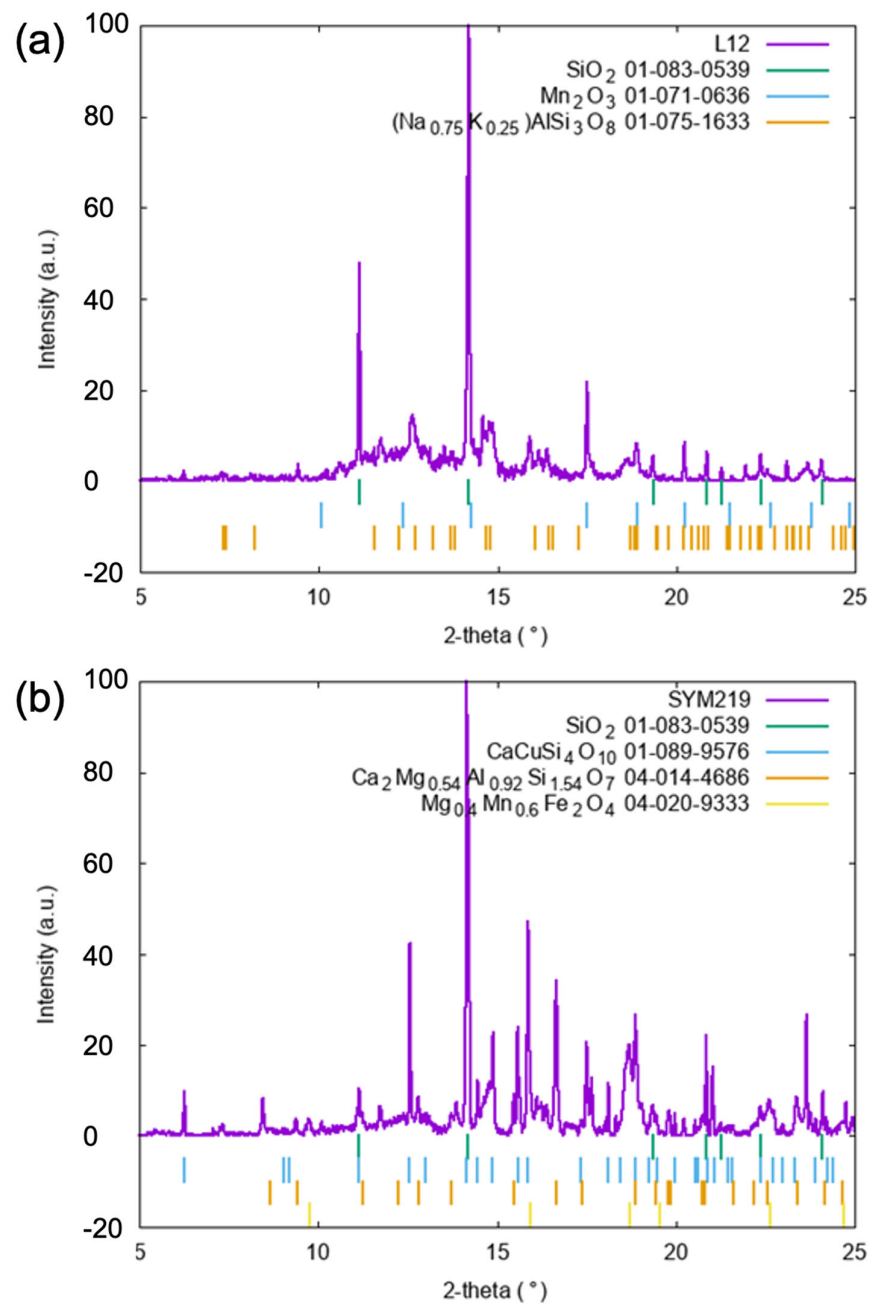


Figure 8. SR-X-ray diffraction pattern collected at the MCX-Elettra Synchrotron Facility on samples (a) L12 and (b) SYM219, as examples of green and blue pigments, respectively.

3. Conclusions

A review of the last decade of synchrotron X-ray applications to cultural heritage summarizes the wide range of applications and methods, highlighting the different types of painted artefacts that can be studied and the challenges of the different techniques, particularly with the benefit of optimized beamlines for cultural heritage materials across Europe. The preparation and handling of the sample, the sample environment, the sample dimensions, the type of study, and the use of different techniques, even at the same point of analysis, all depend on the resolution required for the research goals.

X-ray-based techniques are only a part of the possibilities offered by synchrotron sources for the study of CH materials and, in particular, for the study of pigments and painted surfaces. In fact, other synchrotron-radiation-based techniques such as Fourier-transform infrared (FTIR) and Raman spectroscopies provide complementary information

with respect to X-ray-based methods; for example, FTIR and micro-FTIR spectroscopies (SR-FTIR and SR- μ FTIR) have been used to identify pigments and dyes and study their degradation processes and compounds in easel paints, rock art, and wall paintings [59,66,100–103], as well as to study the coatings of artworks [104]. Additionally, synchrotron radiation Raman spectroscopy (SR-Raman), visible multispectral luminescence microimaging (SR-Deep-UV Excited μ PL), and synchrotron ultraviolet Raman spectroscopy (SR-UV-Raman spectroscopy) have been successfully used for identifying a variety of pigments on different paintings [59,65,105].

The already achieved and the future upgrades of the European synchrotron radiation sources promise improved beamlines and techniques that will certainly help to resolve still complex or unsolved materials science questions.

The presented case studies on Etruscan and Early Roman painted layers from architectural terracottas provided an opportunity to explore the undoubted benefits of integrating techniques and methods to investigate different scientific questions that cannot be answered by traditional approaches. The combination of SR-XRF, SR-XRD, and SR-XANES techniques enabled exploring questions ranging from pigment grains to entire painted layers. Some questions have been resolved while others have opened up new research perspectives. In particular, the possibility of obtaining data at the microscopic level, taking advantage of the high brilliance of synchrotron sources, has provided a more detailed overview of the painting techniques used to obtain different shades, thus enriching the reference studies on the question of the black-manganese technique. It is noteworthy that only a combined approach, including chemical and structural analysis, has been able to trace the ability of Etruscan artisans to manipulate raw materials to obtain specific color effects, claiming the variety of technical solutions developed by the artisans. The research also invites the development of future studies focusing on the black-manganese technique, which could be fundamental for a better understanding of the Etruscan recipes for obtaining, in a single oxidation phase, the different shades of black and red, masterfully combined to create their typical vivid decorative motifs. Overall, the results obtained on the Etruscan and early Roman specimens showed similarities in materiality and pictorial techniques between the two sets of materials, confirming the proposed link between the workshops, namely, a relationship between the Roman slabs and the Etruscan Veii.

Author Contributions: Conceptualization, A.G. and S.R.; data curation, A.G. and S.R.; formal analysis, A.G., S.S., J.R.P. and S.R.; funding acquisition, A.G. and S.R.; investigation, A.G., S.S., J.R.P. and S.R.; methodology, A.G., S.S., J.R.P. and S.R.; writing—original draft, A.G., M.F. and S.R.; writing—review and editing, A.G., S.S., J.R.P., M.F., G.B., A.R., P.M. and S.R. All authors have read and agreed to the published version of the manuscript.

Funding: Part of the results presented within paragraph 2 were carried out at SOLEIL Synchrotron radiation source thanks to financial support by the Access to Research Infrastructures activity in the H2020 Framework Program of the EU (IPERION CH Grant agreement no. 654028).

Data Availability Statement: Original data can be made available upon request.

Acknowledgments: We are grateful to SOLEIL and Elettra synchrotrons for providing access to their facilities and to the beamlines.

Conflicts of Interest: The authors declare no conflicts of interest.

References

1. Cotte, M.; Dollman, K.; Fernandez, V.; Gonzalez, V.; Vanmeert, F.; Monico, L.; Dejoie, C.; Burghammer, M.; Huder, L.; Fisher, S.; et al. New Opportunities Offered by the ESRF to the Cultural and Natural Heritage Communities. *Synchrotron Radiat. News* **2022**, *35*, 3–9. [[CrossRef](#)]
2. Reguer, S.; Schöder, S.; Vantelon, D.; Weitkamp, T.; Rueff, J.-P.; Berenguer, F.; King, A.; Jamme, F.; Hunault, M.O.J.Y.; Silly, M.G.; et al. Fifteen Years of Study of Cultural and Natural Heritage Materials at SOLEIL. *Synchrotron Radiat. News* **2022**, *35*, 10–20. [[CrossRef](#)]
3. Amati, M.; Gianoncelli, A.; Karantzoulis, E.; Rossi, B.; Vaccari, L.; Zanini, F. Looking at Ancient Objects under a Different Light: Cultural Heritage Science at Elettra. *Radiat. Eff. Defects Solids* **2022**, *177*, 1271–1287. [[CrossRef](#)]

4. Cotte, M.; Pouyet, E.; Salomé, M.; Rivard, C.; Nolf, W.D.; Castillo-Michel, H.; Fabris, T.; Monico, L.; Janssens, K.; Wang, T.; et al. The ID21 X-ray and Infrared Microscopy Beamline at the ESRF: Status and Recent Applications to Artistic Materials. *J. Anal. At. Spectrom.* **2017**, *32*, 477–493. [CrossRef]
5. Janssens, K.; Van der Snickt, G.; Vanmeert, F.; Legrand, S.; Nuyts, G.; Alfeld, M.; Monico, L.; Anaf, W.; De Nolf, W.; Vermeulen, M.; et al. Non-Invasive and Non-Destructive Examination of Artistic Pigments, Paints, and Paintings by Means of X-ray Methods. *Top. Curr. Chem.* **2016**, *374*, 81. [CrossRef] [PubMed]
6. Janssens, K.; Cotte, M. Using Synchrotron Radiation for Characterization of Cultural Heritage Materials. In *Synchrotron Light Sources and Free-Electron Lasers*; Springer: Cham, Switzerland, 2020; pp. 2457–2483, ISBN 978-3-030-23200-9.
7. Smieska, L.M.; Woll, A.R.; Vanmeert, F.; Janssens, K. Synchrotron-Based High-Energy X-ray MA-XRF and MA-XRD for Art and Archaeology. *Synchrotron Radiat. News* **2019**, *32*, 29–33. [CrossRef]
8. Cotte, M.; Gonzalez, V.; Vanmeert, F.; Monico, L.; Dejoie, C.; Burghammer, M.; Huder, L.; de Nolf, W.; Fisher, S.; Fazlic, I.; et al. The “Historical Materials BAG”: A New Facilitated Access to Synchrotron X-ray Diffraction Analyses for Cultural Heritage Materials at the European Synchrotron Radiation Facility. *Molecules* **2022**, *27*, 1997. [CrossRef] [PubMed]
9. Cotte, M.; Genty-Vincent, A.; Janssens, K.; Susini, J. Applications of Synchrotron X-ray Nano-Probes in the Field of Cultural Heritage. *C. R. Phys.* **2018**, *19*, 575–588. [CrossRef]
10. Dik, J.; Janssens, K.; Van Der Snickt, G.; van der Loeff, L.; Rickers, K.; Cotte, M. Visualization of a Lost Painting by Vincent van Gogh Using Synchrotron Radiation Based X-ray Fluorescence Elemental Mapping. *Anal. Chem.* **2008**, *80*, 6436–6442. [CrossRef]
11. Gianoncelli, A.; Kourousias, G.; Schöder, S.; Santostefano, A.; L’Héronde, M.; Barone, G.; Mazzoleni, P.; Raneri, S. Synchrotron X-ray Microprobes: An Application on Ancient Ceramics. *Appl. Sci.* **2021**, *11*, 8052. [CrossRef]
12. de Boer, D.K.G. Fundamental Parameters for X-ray Fluorescence Analysis. *Spectrochim. Acta Part B At. Spectrosc.* **1989**, *44*, 1171–1190. [CrossRef]
13. De Boer, D.K.G.; Borstrok, J.J.M.; Leenaers, A.J.G.; Van Sprang, H.A.; Brouwer, P.N. How Accurate Is the Fundamental Parameter Approach? XRF Analysis of Bulk and Multilayer Samples. *X-ray Spectrom.* **1993**, *22*, 33–38. [CrossRef]
14. Handbook of X-ray Spectrometry. Available online: <https://www.routledge.com/Handbook-of-X-ray-Spectrometry/VanGrieken-Markowicz/p/book/9780824706005> (accessed on 19 March 2024).
15. Švarcová, S.; Bezdička, P.; Hradil, D.; Hradilová, J.; Žižak, I. Clay Pigment Structure Characterisation as a Guide for Provenance Determination—A Comparison between Laboratory Powder Micro-XRD and Synchrotron Radiation XRD. *Anal. Bioanal. Chem.* **2011**, *399*, 331–336. [CrossRef] [PubMed]
16. Artioli, G. Science for the Cultural Heritage: The Contribution of X-ray Diffraction. *Rend. Fis. Acc. Lincei* **2013**, *24*, 55–62. [CrossRef]
17. Possenti, E.; Colombo, C.; Conti, C.; Gigli, L.; Merlini, M.; Plaisier, J.R.; Realini, M.; Gatta, G.D. What’s underneath? A Non-Destructive Depth Profile of Painted Stratigraphies by Synchrotron Grazing Incidence X-ray Diffraction. *Analyst* **2018**, *143*, 4290–4297. [CrossRef] [PubMed]
18. Monico, L.; Prati, S.; Sciutto, G.; Catelli, E.; Romani, A.; Balbas, D.Q.; Li, Z.; Meyer, S.D.; Nuyts, G.; Janssens, K.; et al. Development of a Multi-Method Analytical Approach Based on the Combination of Synchrotron Radiation X-ray Micro-Analytical Techniques and Vibrational Micro-Spectroscopy Methods to Unveil the Causes and Mechanism of Darkening of “Fake-Gilded” Decorations in a Cimabue Painting. *J. Anal. At. Spectrom.* **2022**, *37*, 114–129. [CrossRef]
19. Van der Snickt, G.; Janssens, K.; Dik, J.; De Nolf, W.; Vanmeert, F.; Jaroszewicz, J.; Cotte, M.; Falkenberg, G.; Van der Loeff, L. Combined Use of Synchrotron Radiation Based Micro-X-ray Fluorescence, Micro-X-ray Diffraction, Micro-X-ray Absorption Near-Edge, and Micro-Fourier Transform Infrared Spectroscopies for Revealing an Alternative Degradation Pathway of the Pigment Cadmium Yellow in a Painting by Van Gogh. *Anal. Chem.* **2012**, *84*, 10221–10228. [CrossRef] [PubMed]
20. Vanmeert, F.; De Wael, K.; Janssens, K.; Falkenberg, G.; Cotte, M. Using Synchrotron Radiation for Understanding the Spontaneous Degradation of Artists’ Pigments. *Synchrotron Radiat. News* **2019**, *32*, 41–47. [CrossRef]
21. Huntley, J.; Brand, H.; Aubert, M.; Morwood, M. The First Australian Synchrotron Powder Diffraction Analysis of Pigment from a Wandjina Motif in the Kimberley, Western Australia. *Aust. Archaeol.* **2014**, *78*, 33. [CrossRef]
22. Gay, M.; Alfeld, M.; Menu, M.; Laval, E.; Arias, P.; Ontañón, R.; Reiche, I. Palaeolithic Paint Palettes Used at La Garma Cave (Cantabria, Spain) Investigated by Means of Combined in Situ and Synchrotron X-ray Analytical Methods. *J. Anal. At. Spectrom.* **2015**, *30*, 767–776. [CrossRef]
23. Ilimi, M.M.; Nurdini, N.; Maryanti, E.; Saiyasombat, C.; Setiawan, P.; Kadja, G.T.M. Ismunandar Multi-Analytical Characterizations of Prehistoric Rock Art Pigments from Karim Cave, Sangkulirang–Mangkalihat Site, East Kalimantan, Indonesia. *Microchem. J.* **2020**, *155*, 104738. [CrossRef]
24. Maryanti, E.; Ilimi, M.M.; Nurdini, N.; Setiawan, P.; Syah, Y.M.; Saiyasombat, C.; Kadja, G.T.M. Ismunandar Hematite as Unprecedented Black Rock Art Pigment in Jufri Cave, East Kalimantan, Indonesia: The Microscopy, Spectroscopy, and Synchrotron X-ray-Based Investigation. *Archaeol. Anthr. Sci.* **2022**, *14*, 122. [CrossRef]
25. Nurdini, N.; Maryanti, E.; Ilimi, M.M.; Setiawan, P.; Saiyasombat, C.; Kadja, G.T.M. Ismunandar Physicochemical Investigation of Prehistoric Rock Art Pigments in Tewet Cave, Sangkulirang–Mangkalihat Site, East Kalimantan-Indonesia. *J. Archaeol. Sci. Rep.* **2020**, *31*, 102345. [CrossRef]
26. Debastiani, R.; Simon, R.; Batchelor, D.; Dellagustin, G.; Baumbach, T.; Fiederle, M. Synchrotron-Based Scanning Macro-X-ray Fluorescence Applied to Fragments of Roman Mural Paintings. *Microchem. J.* **2016**, *126*, 438–445. [CrossRef]

27. Bugoi, R.; Constantinescu, B.; Pantos, E.; Popovici, D. Investigation of Neolithic Ceramic Pigments Using Synchrotron Radiation X-ray Diffraction. *Powder Diffr.* **2008**, *23*, 195–199. [[CrossRef](#)]
28. Jones, R. The Decoration and Firing of Ancient Greek Pottery: A Review of Recent Investigations. *Adv. Archaeomater.* **2021**, *2*, 67–127. [[CrossRef](#)]
29. Wang, T.; Zhu, T.Q.; Feng, Z.Y.; Fayard, B.; Pouyet, E.; Cotte, M.; De Nolf, W.; Salomé, M.; Sciau, P. Synchrotron Radiation-Based Multi-Analytical Approach for Studying Underglaze Color: The Microstructure of Chinese Qinghua Blue Decors (Ming Dynasty). *Anal. Chim. Acta* **2016**, *928*, 20–31. [[CrossRef](#)]
30. Pradell, T.; Fernandes, R.; Molina, G.; Smith, A.D.; Molera, J.; Climent-Font, A.; Tite, M.S. Technology of Production of Syrian Lustre (11th to 13th Century). *J. Eur. Ceram. Soc.* **2018**, *38*, 2716–2727. [[CrossRef](#)]
31. Molera, J.; Colomer, M.; Vallcorba, O.; Pradell, T. Manganese Crystalline Phases Developed in High Lead Glazes during Firing. *J. Eur. Ceram. Soc.* **2022**, *42*, 4006–4015. [[CrossRef](#)]
32. Molera, J.; Climent-Font, A.; Garcia, G.; Pradell, T.; Vallcorba, O.; Zucchiatti, A. Experimental Study of Historical Processing of Cobalt Arsenide Ore for Colouring Glazes (15–16th Century Europe). *J. Archaeol. Sci. Rep.* **2021**, *36*, 102797. [[CrossRef](#)]
33. Di Febo, R.; Casas, L.; del Campo, Á.A.; Rius, J.; Vallcorba, O.; Melgarejo, J.C.; Capelli, C. Recognizing and Understanding Silica-Polymorph Microcrystals in Ceramic Glazes. *J. Eur. Ceram. Soc.* **2020**, *40*, 6188–6199. [[CrossRef](#)]
34. Di Febo, R.; Casas, L.; Rius, J.; Tagliapietra, R.; Melgarejo, J.C. Breaking Preconceptions: Thin Section Petrography For Ceramic Glaze Microstructures. *Minerals* **2019**, *9*, 113. [[CrossRef](#)]
35. Febo, R.D.; Molera, J.; Pradell, T.; Vallcorba, O.; Melgarejo, J.C.; Capelli, C. Thin-Section Petrography and SR- μ XRD for the Identification of Micro-Crystallites in the Brown Decorations of Ceramic Lead Glazes. *Eur. J. Miner.* **2017**, *29*, 861–870. [[CrossRef](#)]
36. Coentro, S.; Alves, L.C.; Relvas, C.; Ferreira, T.; Mirão, J.; Molera, J.; Pradell, T.; Trindade, R.A.A.; Da Silva, R.C.; Muralha, V.S.F. The Glaze Technology of Hispano-Moresque Ceramic Tiles: A Comparison between Portuguese and Spanish Collections. *Archaeometry* **2017**, *59*, 667–684. [[CrossRef](#)]
37. Roqué-Rosell, J.; Pinto, A.; Marini, C.; Prieto Burgos, J.; Groenen, J.; Campeny, M.; Sciau, P. Synchrotron XAS Study of Mn and Fe in Chinese Blue-and-White Ming Porcelains from the Second Half of the 15th Century. *Ceram. Int.* **2021**, *47*, 2715–2724. [[CrossRef](#)]
38. Zhu, J.; Zhang, J.; Chen, G.; Du, J.; Li, W.; Li, Y. The Application of Confocal Depth-Resolved Micro-X-ray Absorption Spectroscopy to Study Colorant Copper in Ancient Lead-Silica Glassy System at the Beijing Synchrotron Radiation Facility. *Optik* **2020**, *218*, 165239. [[CrossRef](#)]
39. Verger, L.; Dargaud, O.; Chassé, M.; Trcera, N.; Rousse, G.; Cormier, L. Synthesis, Properties and Uses of Chromium-Based Pigments from the Manufacture de Sèvres. *J. Cult. Herit.* **2018**, *30*, 26–33. [[CrossRef](#)]
40. De Pauw, E.; Tack, P.; Verhaeven, E.; Bauters, S.; Acke, L.; Vekemans, B.; Vincze, L. Microbeam X-ray Fluorescence and X-ray Absorption Spectroscopic Analysis of Chinese Blue-and-White Kraak Porcelain Dating from the Ming Dynasty. *Spectrochim. Acta Part B At. Spectrosc.* **2018**, *149*, 190–196. [[CrossRef](#)]
41. Li, Y.; Zhu, J.; Ji, L.; Shan, Y.; Jiang, S.; Chen, G.; Sciau, P.; Wang, W.; Wang, C. Study of Arsenic in *Famille Rose* Porcelain from the Imperial Palace of Qing Dynasty, Beijing, China. *Ceram. Int.* **2018**, *44*, 1627–1632. [[CrossRef](#)]
42. Wen, R.; Wang, D.; Wang, L.; Dang, Y. The Colouring Mechanism of the Brown Glaze Porcelain of the Yaozhou Kiln in the Northern Song Dynasty. *Ceram. Int.* **2019**, *45*, 10589–10595. [[CrossRef](#)]
43. Yuan, M.; Hou, J.; Gorni, G.; Crespo, D.; Li, Y.; Pradell, T. Jun Ware Glaze Colours: An X-ray Absorption Spectroscopy Study. *J. Eur. Ceram. Soc.* **2022**, *42*, 3015–3022. [[CrossRef](#)]
44. Jia, C.; Li, G.; Guan, M.; Zhao, J.; Zheng, Y.; Wang, G.; Wei, X.; Lei, Y. A Short but Glorious Porcelain Glaze of Early Ming Dynasty: New Finding of Raw Material and Colorants in the Copper Red Glaze. *J. Eur. Ceram. Soc.* **2021**, *41*, 3809–3815. [[CrossRef](#)]
45. Gianoncelli, A.; Raneri, S.; Schoeder, S.; Okbinoglu, T.; Barone, G.; Santostefano, A.; Mazzoleni, P. Synchrotron M-XRF Imaging and μ -XANES of Black-Glazed Wares at the PUMA Beamline: Insights on Technological Markers for Colonial Productions. *Microchem. J.* **2020**, *154*, 104629. [[CrossRef](#)]
46. Dejoie, C.; Sciau, P.; Li, W.; Noé, L.; Mehta, A.; Chen, K.; Luo, H.; Kunz, M.; Tamura, N.; Liu, Z. Learning from the Past: Rare ϵ -Fe₂O₃ in the Ancient Black-Glazed Jian (Tenmoku) Wares. *Sci. Rep.* **2014**, *4*, 4941. [[CrossRef](#)]
47. Burgio, L. Pigments, Dyes and Inks: Their Analysis on Manuscripts, Scrolls and Papyri. *Archaeol. Anthr. Sci.* **2021**, *13*, 194. [[CrossRef](#)]
48. Christiansen, T.; Cotte, M.; Loredó-Portales, R.; Lindelof, P.E.; Mortensen, K.; Ryholt, K.; Larsen, S. The Nature of Ancient Egyptian Copper-Containing Carbon Inks Is Revealed by Synchrotron Radiation Based X-ray Microscopy. *Sci. Rep.* **2017**, *7*, 15346. [[CrossRef](#)] [[PubMed](#)]
49. Christiansen, T.; Cotte, M.; de Nolf, W.; Mouro, E.; Reyes-Herrera, J.; de Meyer, S.; Vanmeert, F.; Salvadó, N.; Gonzalez, V.; Lindelof, P.E.; et al. Insights into the Composition of Ancient Egyptian Red and Black Inks on Papyri Achieved by Synchrotron-Based Microanalyses. *Proc. Natl. Acad. Sci. USA* **2020**, *117*, 27825–27835. [[CrossRef](#)] [[PubMed](#)]
50. Autran, P.-O.; Dejoie, C.; Bordet, P.; Hodeau, J.-L.; Dugand, C.; Gervason, M.; Anne, M.; Martinetto, P. Revealing the Nature of Black Pigments Used on Ancient Egyptian Papyri from Champollion Collection. *Anal. Chem.* **2021**, *93*, 1135–1142. [[CrossRef](#)] [[PubMed](#)]
51. Smieska, L.M.; Mullett, R.; Ferri, L.; Woll, A.R. Trace Elements in Natural Azurite Pigments Found in Illuminated Manuscript Leaves Investigated by Synchrotron X-ray Fluorescence and Diffraction Mapping. *Appl. Phys. A* **2017**, *123*, 484. [[CrossRef](#)]

52. Arlt, T.; Mahnke, H.-E.; Siopi, T.; Menei, E.; Aibéo, C.; Pausewein, R.-R.; Reiche, I.; Manke, I.; Lepper, V. Absorption Edge Sensitive Radiography and Tomography of Egyptian Papyri. *J. Cult. Herit.* **2019**, *39*, 13–20. [[CrossRef](#)]
53. Pouyet, E.; Devine, S.; Grafakos, T.; Kieckhefer, R.; Salvant, J.; Smieska, L.; Woll, A.; Katsaggelos, A.; Cossairt, O.; Walton, M. Revealing the Biography of a Hidden Medieval Manuscript Using Synchrotron and Conventional Imaging Techniques. *Anal. Chim. Acta* **2017**, *982*, 20–30. [[CrossRef](#)] [[PubMed](#)]
54. Späth, A.; Meyer, M.; Huthwelker, T.; Borca, C.N.; Meßlinger, K.; Bieber, M.; Barkova, L.L.; Fink, R.H. X-ray Microscopy Reveals the Outstanding Craftsmanship of Siberian Iron Age Textile Dyers. *Sci. Rep.* **2021**, *11*, 5141. [[CrossRef](#)] [[PubMed](#)]
55. Borg, B.; Dunn, M.; Ang, A.; Villis, C. The Application of State-of-the-Art Technologies to Support Artwork Conservation: Literature Review. *J. Cult. Herit.* **2020**, *44*, 239–259. [[CrossRef](#)]
56. Dalecky, L.; Bonaduce, I.; Anheim, É.; Nasa, J.L.; L'heronde, M.; Morel, C.; Catelli, E.; Prati, S.; Li, Z.; Beck, L.; et al. A Typical Postwar Workshop: Insights into Simon Hantaï's Oil Paint Palette. *J. Cult. Herit.* **2024**, *66*, 511–522. [[CrossRef](#)]
57. Gonzalez, V.; Wallez, G.; Calligaro, T.; Cotte, M.; De Nolf, W.; Eveno, M.; Ravaud, E.; Menu, M. Synchrotron-Based High Angle Resolution and High Lateral Resolution X-ray Diffraction: Revealing Lead White Pigment Qualities in Old Masters Paintings. *Anal. Chem.* **2017**, *89*, 13203–13211. [[CrossRef](#)] [[PubMed](#)]
58. Miliani, C.; Monico, L.; Melo, M.J.; Fantacci, S.; Angelin, E.M.; Romani, A.; Janssens, K. Photochemistry of Artists' Dyes and Pigments: Towards Better Understanding and Prevention of Colour Change in Works of Art. *Angew. Chem. Int. Ed.* **2018**, *57*, 7324–7334. [[CrossRef](#)] [[PubMed](#)]
59. Monico, L.; Janssens, K.; Hendriks, E.; Vanmeert, F.; Van der Snickt, G.; Cotte, M.; Falkenberg, G.; Brunetti, B.G.; Miliani, C. Evidence for Degradation of the Chrome Yellows in Van Gogh's Sunflowers: A Study Using Noninvasive In Situ Methods and Synchrotron-Radiation-Based X-ray Techniques. *Angew. Chem. Int. Ed.* **2015**, *54*, 13923–13927. [[CrossRef](#)] [[PubMed](#)]
60. Monico, L.; Janssens, K.; Cotte, M.; Sorace, L.; Vanmeert, F.; Brunetti, B.G.; Miliani, C. Chromium Speciation Methods and Infrared Spectroscopy for Studying the Chemical Reactivity of Lead Chromate-Based Pigments in Oil Medium. *Microchem. J.* **2016**, *124*, 272–282. [[CrossRef](#)]
61. Monico, L.; Cartechini, L.; Rosi, F.; Chieli, A.; Grazia, C.; De Meyer, S.; Nuyts, G.; Vanmeert, F.; Janssens, K.; Cotte, M.; et al. Probing the Chemistry of CdS Paints in The Scream by in Situ Noninvasive Spectroscopies and Synchrotron Radiation X-ray Techniques. *Sci. Adv.* **2020**, *6*, eaay3514. [[CrossRef](#)]
62. Monico, L.; Cotte, M.; Vanmeert, F.; Amidani, L.; Janssens, K.; Nuyts, G.; Garrevoet, J.; Falkenberg, G.; Glatzel, P.; Romani, A.; et al. Damages Induced by Synchrotron Radiation-Based X-ray Microanalysis in Chrome Yellow Paints and Related Cr-Compounds: Assessment, Quantification, and Mitigation Strategies. *Anal. Chem.* **2020**, *92*, 14164–14173. [[CrossRef](#)]
63. Pouyet, E.; Fayard, B.; Salomé, M.; Taniguchi, Y.; Sette, F.; Cotte, M. Thin-Sections of Painting Fragments: Opportunities for Combined Synchrotron-Based Micro-Spectroscopic Techniques. *Herit. Sci.* **2015**, *3*, 3. [[CrossRef](#)]
64. Bronken, I.A.T.; Boon, J.J.; Corkery, R.; Steindal, C.C. Changing Surface Features, Weeping and Metal Soap Formation in Paintings by Karel Appel and Asger Jorn from 1946–1971. *J. Cult. Herit.* **2019**, *35*, 279–287. [[CrossRef](#)]
65. Ghirardello, M.; Gonzalez, V.; Monico, L.; Nevin, A.; MacLennan, D.; Patterson, C.S.; Burghammer, M.; Réfrégiers, M.; Comelli, D.; Cotte, M. Application of Synchrotron Radiation-Based Micro-Analysis on Cadmium Yellows in Pablo Picasso's Femme. *Microsc. Microanal.* **2022**, *28*, 1504–1513. [[CrossRef](#)]
66. Salvadó, N.; Butí, S.; Aranda, M.A.G.; Pradell, T. New Insights on Blue Pigments Used in 15th Century Paintings by Synchrotron Radiation-Based Micro-FTIR and XRD. *Anal. Methods* **2014**, *6*, 3610–3621. [[CrossRef](#)]
67. Monico, L.; d'Acapito, F.; Cotte, M.; Janssens, K.; Romani, A.; Ricci, G.; Miliani, C.; Cartechini, L. Total Electron Yield (TEY) Detection Mode Cr K-Edge XANES Spectroscopy as a Direct Method to Probe the Composition of the Surface of Darkened Chrome Yellow (PbCr_{1-x}SxO₄) and Potassium Chromate Paints. *Nucl. Instrum. Methods Phys. Res. Sect. B Beam Interact. Mater. At.* **2023**, *539*, 141–147. [[CrossRef](#)]
68. Ganio, M.; Pouyet, E.S.; Webb, S.M.; Schmidt Patterson, C.M.; Walton, M.S. From Lapis Lazuli to Ultramarine Blue: Investigating Cennino Cennini's Recipe Using Sulfur K-Edge XANES. *Pure Appl. Chem.* **2018**, *90*, 463–475. [[CrossRef](#)]
69. Cato, E.; Borca, C.; Huthwelker, T.; Ferreira, E.S.B. Aluminium X-ray Absorption near-Edge Spectroscopy Analysis of Discoloured Ultramarine Blue in 20th Century Oil Paintings. *Microchem. J.* **2016**, *126*, 18–24. [[CrossRef](#)]
70. Gonzalez, V.; Calligaro, T.; Wallez, G.; Eveno, M.; Toussaint, K.; Menu, M. Composition and microstructure of the lead white pigment in Masters paintings using HR Synchrotron XRD. *Microchem. J.* **2016**, *125*, 43–49. [[CrossRef](#)]
71. Vermeulen, M.; Janssens, K.; Sanyova, J.; Rahemi, V.; McGlinchey, C.; De Wael, K. Assessing the Stability of Arsenic Sulfide Pigments and Influence of the Binding Media on Their Degradation by Means of Spectroscopic and Electrochemical Techniques. *Microchem. J.* **2018**, *138*, 82–91. [[CrossRef](#)]
72. Fanost, A.; Gimat, A.; de Viguier, L.; Martinetto, P.; Giot, A.-C.; Clémancey, M.; Blondin, G.; Gaslain, F.; Glanville, H.; Walter, P.; et al. Revisiting the Identification of Commercial and Historical Green Earth Pigments. *Colloids Surf. A Physicochem. Eng. Asp.* **2020**, *584*, 124035. [[CrossRef](#)]
73. Dredge, P.; Ives, S.; Howard, D.L.; Spiers, K.M.; Yip, A.; Kenderdine, S. Mapping Henry: Synchrotron-Sourced X-ray Fluorescence Mapping and Ultra-High-Definition Scanning of an Early Tudor Portrait of Henry VIII. *Appl. Phys. A* **2015**, *121*, 789–800. [[CrossRef](#)]
74. Pouyet, E.; Lluveras-Tenorio, A.; Nevin, A.; Saviello, D.; Sette, F.; Cotte, M. Preparation of Thin-Sections of Painting Fragments: Classical and Innovative Strategies. *Anal. Chim. Acta* **2014**, *822*, 51–59. [[CrossRef](#)] [[PubMed](#)]

75. Pereira, M.O.; Felix, V.S.; Oliveira, A.L.; Ferreira, D.S.; Pimenta, A.R.; Carvalho, C.S.; Silva, F.L.; Perez, C.A.; Galante, D.; Freitas, R.P. Investigating Counterfeiting of an Artwork by XRF, SEM-EDS, FTIR and Synchrotron Radiation Induced MA-XRF at LNLS-BRAZIL. *Spectrochim. Acta Part A Mol. Biomol. Spectrosc.* **2021**, *246*, 118925. [[CrossRef](#)] [[PubMed](#)]
76. Smieska, L.M.; Twilley, J.; Woll, A.R.; Schafer, M.; Marcereau DeGalan, A. Energy-Optimized Synchrotron XRF Mapping of an Obscured Painting beneath *Exit from the Theater*, Attributed to Honoré Daumier. *Microchem. J.* **2019**, *146*, 679–691. [[CrossRef](#)]
77. Oriols, N.; Salvadó, N.; Pradell, T.; Jiménez, N.; Juanhuix, J.; Butí, S. The Three-Tone System in Sant Climent de Taüll Wall Paintings: An Imprint of Medieval Treatises. *J. Cult. Herit.* **2023**, *62*, 114–123. [[CrossRef](#)]
78. Alfeld, M.; de Viguierie, L. Recent Developments in Spectroscopic Imaging Techniques for Historical Paintings—A Review. *Spectrochim. Acta* **2017**, *136*, 81–105. [[CrossRef](#)]
79. Vandenabeele, P.; Donais, M.K. Mobile Spectroscopic Instrumentation in Archaeometry Research. *Appl. Spectrosc.* **2016**, *70*, 27–41. [[CrossRef](#)] [[PubMed](#)]
80. Bertrand, L.; Schoeder, S.; Anglos, D.; Breese, M.B.H.; Janssens, K.; Moini, M.; Simon, A. Mitigation Strategies for Radiation Damage in the Analysis of Ancient Materials. *Trends Anal. Chem.* **2015**, *66*, 128–145. [[CrossRef](#)]
81. Bertrand, L.; Schöder, S.; Joosten, I.; Webb, S.M.; Thoury, M.; Calligaro, T.; Anheim, É.; Simon, A. Practical Advances towards Safer Analysis of Heritage Samples and Objects. *TrAC Trends Anal. Chem.* **2023**, *164*, 117078. [[CrossRef](#)]
82. Godet, M.; Binet, L.; Schöder, S.; Brunel-Duverger, L.; Thoury, M.; Bertrand, L. X-ray Irradiation Effects on Egyptian Blue and Green Pigments. *J. Anal. At. Spectrom.* **2022**, *37*, 1265–1272. [[CrossRef](#)]
83. Gervais, C.; Thoury, M.; Réguer, S.; Gueriau, P.; Mass, J. Radiation Damages during Synchrotron X-ray Micro-Analyses of Prussian Blue and Zinc White Historic Paintings: Detection, Mitigation and Integration. *Appl. Phys. A* **2015**, *121*, 949–955. [[CrossRef](#)]
84. Carrasco, E.; Oujja, M.; Sanz, M.; Marco, J.F.; Castillejo, M. X-ray and Ion Irradiation Effects on Azurite, Malachite and Alizarin Pictorial Models. *Microchem. J.* **2018**, *137*, 381–391. [[CrossRef](#)]
85. Barone, G.; Fugazzotto, M.; Mazzoleni, P.; Raneri, S.; Russo, A. Color and Painting Techniques in Etruscan Architectural Slabs. *Dyes Pigment.* **2019**, *171*, 107766. [[CrossRef](#)]
86. Fugazzotto, M.; Stroschio, A.; Mazzoleni, P.; Panella, C.; Russo, A.; Raneri, S.; Barone, G. Ceramic Technology and Paintings of Archaic Architectural Slabs, Louteria and Antefixes from the Palatine Hill in Rome (Italy). *Archaeometry* **2022**, *64*, 118–133. [[CrossRef](#)]
87. Plaisier, J.R.; Nodari, L.; Gigli, L.; Miguel, E.P.R.S.; Bertinello, R.; Lausi, A. The X-ray Diffraction Beamline MCX at Elettra: A Case Study of Non-Destructive Analysis on Stained Glass. *Acta IMEKO* **2017**, *6*, 71–75. [[CrossRef](#)]
88. Cosentino, R.; Russo, A.; Zaccagnini, R. (Eds.) *Pittura di Terracotta: Mito e Immagine Nelle Lastre Dipinte di Cerveteri*; Gangemi Editore: Rome, Italy, 2018; ISBN 978-88-492-3632-3.
89. Barone, G.; Mazzoleni, P.; Cecchini, A.; Russo, A. In Situ Raman and pXRF Spectroscopic Study on the Wall Paintings of Etruscan Tarquinia Tombs. *Dyes Pigment.* **2018**, *150*, 390–403. [[CrossRef](#)]
90. Guidi, G.F.; Bellelli, V.; Trojsi, G. *Il Guerriero di Ceri: Tecnologie per far Rivivere e Interpretare un Capolavoro della Pittura Etrusca su Terracotta*; Guidi, G.F., Bellelli, V., Trojsi, G., Eds.; ENEA: Rome, Italy, 2006; ISBN 978-88-8286-195-7.
91. Gates-Rector, S.; Blanton, T. The Powder Diffraction File: A Quality Materials Characterization Database. *Powder Diffr.* **2019**, *34*, 352–360. [[CrossRef](#)]
92. Schweizer, F.; Rinuy, A. Manganese Black as an Etruscan Pigment. *Stud. Conserv.* **1982**, *27*, 118–123. [[CrossRef](#)]
93. Bordignon, F.; Postorino, P.; Dore, P.; Trojsi, G. Raman Identification of Green and Blue Pigments in Etruscan Polychromes on Architectural Terracotta Panels. *J. Raman Spectrosc.* **2007**, *38*, 255–259. [[CrossRef](#)]
94. Vermeersch, E.; Pincé, P.; Jehlička, J.; Culka, A.; Rousaki, A.; Vandenabeele, P. Micro-Raman Spectroscopy on Pigments of Painted pre-Islamic Ceramics from the Kur River Basin (Fars Province, Iran): The Case of Manganese Oxides Identification. *J. Raman Spectrosc.* **2022**, *53*, 1402–1414. [[CrossRef](#)]
95. Bernardini, S.; Bellatreccia, F.; Casanova Municchia, A.; Della Ventura, G.; Sodo, A. Raman Spectra of Natural Manganese Oxides. *J. Raman Spectrosc.* **2019**, *50*, 873–888. [[CrossRef](#)]
96. Bernardini, S.; Bellatreccia, F.; Della Ventura, G.; Sodo, A. A Reliable Method for Determining the Oxidation State of Manganese at the Microscale in Mn Oxides via Raman Spectroscopy. *Geostand. Geoanal. Res.* **2021**, *45*, 223–244. [[CrossRef](#)]
97. Jorge-Villar, S.E.; Edwards, H.G.M. Green and Blue Pigments in Roman Wall Paintings: A Challenge for Raman Spectroscopy. *J. Raman Spectrosc.* **2021**, *52*, 2190–2203. [[CrossRef](#)]
98. Wiggins, M.B.; Alcántara-García, J.; Booksh, K.S. Characterization of Copper-Based Pigment Preparation and Alteration Products. *MRS Adv.* **2017**, *2*, 3973–3981. [[CrossRef](#)]
99. Coccato, A.; Bersani, D.; Coudray, A.; Sanyova, J.; Moens, L.; Vandenabeele, P. Raman Spectroscopy of Green Minerals and Reaction Products with an Application in Cultural Heritage Research. *J. Raman Spectrosc.* **2016**, *47*, 1429–1443. [[CrossRef](#)]
100. Hunt, A.M.W.; Speakman, R.J. Portable XRF Analysis of Archaeological Sediments and Ceramics. *J. Archaeol. Sci.* **2015**, *53*, 626–638. [[CrossRef](#)]
101. Anderson, E.; Almond, M.J.; Matthews, W.; Cinque, G.; Frogley, M.D. Analysis of Red Pigments from the Neolithic Sites of Çatalhöyük in Turkey and Sheikh-e Abad in Iran. *Spectrochim. Acta Part A Mol. Biomol. Spectrosc.* **2014**, *131*, 373–383. [[CrossRef](#)] [[PubMed](#)]
102. Sabatini, F.; Eis, E.; Degano, I.; Thoury, M.; Bonaduce, I.; Lluveras-Tenorio, A. The Issue of Eosin Fading: A Combined Spectroscopic and Mass Spectrometric Approach Applied to Historical Lakes. *Dyes Pigment.* **2020**, *180*, 108436. [[CrossRef](#)]

103. Pronti, L.; Romani, M.; Viviani, G.; Stani, C.; Gioia, P.; Cestelli-Guidi, M. Advanced Methods for the Analysis of Roman Wall Paintings: Elemental and Molecular Detection by Means of Synchrotron FT-IR and SEM Micro-Imaging Spectroscopy. *Rend. Fis. Acc. Lincei* **2020**, *31*, 485–493. [[CrossRef](#)]
104. Beltran, V.; Salvadó, N.; Butí, S.; Cinque, G. Micro Infrared Spectroscopy Discrimination Capability of Compounds in Complex Matrices of Thin Layers in Real Sample Coatings from Artworks. *Microchem. J.* **2015**, *118*, 115–123. [[CrossRef](#)]
105. Crupi, V.; Allodi, V.; Bottari, C.; D'Amico, F.; Galli, G.; Gessini, A.; Russa, M.F.L.; Longo, F.; Majolino, D.; Mariotto, G.; et al. Spectroscopic Investigation of Roman Decorated Plasters by Combining FT-IR, Micro-Raman and UV-Raman Analyses. *Vib. Spectrosc.* **2016**, *83*, 78–84. [[CrossRef](#)]

Disclaimer/Publisher's Note: The statements, opinions and data contained in all publications are solely those of the individual author(s) and contributor(s) and not of MDPI and/or the editor(s). MDPI and/or the editor(s) disclaim responsibility for any injury to people or property resulting from any ideas, methods, instructions or products referred to in the content.